Research in Astron. Astrophys. Vol.0 (200x) No.0, 000–000
http://www.raa-journal.org *http://www.iop.org/journals/raa*

***R**esearch in*
***A**stronomy and*
***A**strophysics*

arXiv:1401.5659v2 [astro-ph.HE] 19 Nov 2015

Constraints on black hole spins with a general relativistic accretion disk corona model

Bei You[1,3], Xinwu Cao[1], and Ye-Fei Yuan[2]

[1] Key Laboratory for Research in Galaxies and Cosmology, Shanghai Astronomical Observatory, Chinese Academy of Sciences, 80 Nandan Road, Shanghai, 200030, China; *youbeiyb@gmail.com*, *cxw@shao.ac.cn*
[2] Department of Astronomy, University of Sciences and Technology of China, Hefei, Anhui 230026, China; *yfyuan@ustc.edu.cn*
[3] University of Chinese Academy of Sciences, 19A Yuquanlu, Beijing 100049, China

Abstract The peaks of the spectra of the accretion disks surrounding massive black holes in quasars are in the far-UV or soft X-ray band, which are usually not observed. However, in the disk corona model, the soft photons from the disk are Comptonized to high energy in the hot corona, and the hard X-ray spectra (luminosity and spectral shape) contain the information of the incident spectra from the disk. The values of black hole spin parameter a_* are inferred from the spectral fitting, which spread over a large range, ~ -0.94 to 0.998. We find that the inclination angles and mass accretion rates are well determined by the spectral fitting, while the results are sensitive to the accuracy of black hole mass estimates. No tight constraints on the black hole spins are achieved, if the uncertainties of black hole mass measurements are a factor of four, which are typical for the single-epoch reverberation mapping method. Recently, the accuracy of black hole mass measurement has been significantly improved to $0.2-0.4$ dex with velocity resolved reverberation mapping method(Pancoast et al., 2014). The black hole spin can be well constrained if the mass measurement accuracy is $\lesssim 50\%$. In the accretion disk corona scenario, a fraction of power dissipated in the disk is transported into the corona, and therefore the accretion disk is thinner than a bare disk for the same mass accretion rate, because the radiation pressure in the disk is reduced. We find that the thin disk approximation, $H/R \lesssim 0.1$, is still valid if $0.3 < \dot{m} < 0.5$, provided a half of the dissipated power is radiated in the corona above the disk.

Key words: Quasars: accretion disk; X-ray: corona; Black hole physics; Galaxies: active

1 INTRODUCTION

It is believed that black holes reside in X-ray binaries and active galactic nuclei (AGN) with typical masses $\sim 10M_\odot$ and $10^6-10^9M_\odot$ respectively (Kormendy & Richstone, 1995; Ferrarese & Merritt, 2000; Remillard & McClintock, 2006; Hopkins et al., 2008; Alexander & Hickox, 2012). Massive black holes may grow up through gas accretion or/and mergers, which is also related with the galaxy evolution (e.g., Moderski & Sikora, 1996; Marconi et al., 2004; Volonteri et al., 2005; Berti & Volonteri, 2008; Dotti et al., 2013). The structure and radiation of accretion disks surrounding black holes have been extensively studied in the last several decades (Shakura & Sunyaev, 1973; Frank et al., 1992; Merloni, 2004). Relativistic jets have been observed in some X-ray binaries and AGNs, which is thought to be

related to accretion disks or/and spinning black holes (Blandford & Znajek, 1977; Blandford & Payne, 1982).

A black hole can be described by two quantities: the mass M and the dimensionless spin parameter $a_* = cJ/GM^2$, where J is the angular momentum of the black hole. In the last decade, great progresses have been achieved on the mass measurement of black holes in either active or nonactive galaxies. The black hole mass in nearby galaxies can be estimated with the correlations between black hole mass and the stellar velocity dispersion or bulge luminosity of the host galaxy (Kormendy & Richstone, 1995; Ferrarese & Merritt, 2000; McConnell et al., 2011). For active galaxies, the size of the broad-line region (BLR) is measured with reverberation mapping method, and the black hole mass can be estimated with the broad-line width assuming the motion of BLR clouds to be virialized (Kaspi et al., 2000). There is a tight correlation between the BLR size and the optical continuum luminosity, which is widely used to estimate masses of black holes in AGNs, or called as single epoch reverberation mapping method (e.g., Kaspi et al., 2000; Woo & Urry, 2002; Shen et al., 2011; Tang et al., 2012).

Compared with the mass estimates, the measurements of the black hole spins are still far from satisfactory, though great efforts have been devoted on this issue. The observed broad Fe Kα emission lines provide a way to estimate the black hole spin parameters, which is applicable for black holes in both galactic X-ray binaries and AGNs. The observed broad Fe Kα emission lines are believed to be emitted from the inner regions of the accretion disks. The radii of the innermost stable circular orbits (ISCO) of the gas in the accretion disks can be inferred from the observed asymmetric Fe kα line profiles (Martocchia et al., 2002; Miller et al., 2002; Miniutti et al., 2004; Brenneman & Reynolds, 2006; Lohfink et al., 2012), and the dimensionless spin a_* can be determined with the radii of the ISCO (Barr et al., 1985; Reynolds & Nowak, 2003; Remillard & McClintock, 2006). The application of this method requires high quality X-ray spectroscopic data, and a few black hole spins in nearby Seyfert galaxies have been measured in this way (Goosmann et al., 2006; Brenneman & Reynolds, 2006; de La Calle Pérez et al., 2010; Patrick et al., 2011; Lohfink et al., 2012).

The black hole spin parameters in some X-ray binaries were measured by fitting the observed continuum spectra with general relativistic accretion disk models (so-called "continuum-fitting method", Zhang et al., 1997; Shafee et al., 2006; Steiner et al., 2009a; Gou et al., 2011; McClintock et al., 2011; You et al., 2015). In principle, this method can be used to constrain the black hole spins for AGNs. In some early works, the accretion disk models were used to fit the observed multi-band spectra of quasars (e.g., Bechtold et al., 1987; Sun & Malkan, 1989), in which the general relativistic effects have been taken into account (Cunningham, 1975; Laor, 1991). Czerny et al. (2011) estimated the black hole spin to be $a_* = 0.3$ by fitting the broad band (IR/optical/UV) continuum spectrum of the quasar SDSS J094533.99+100950.1. It was found that the model fitting suffers from the degeneracy of the disk parameters, namely, the black hole mass M, the spin a_*, and the mass accretion rate $\dot{M}$. At the time before the invention of the black hole mass measurements used nowadays, the derived disk parameters with the spectral fittings are quite uncertain. It is possible to constrain the the spins of the massive black holes in AGNs, when the black hole masses are measured. The degeneracy of the parameters in accretion disk spectral fittings can be eliminated if the peak frequency and luminosity of the accretion disk are well observed. However, the application of this method in AGNs meets a major difficulty, i.e., the spectral peaks of accretion disks surrounding massive black holes with $\sim 10^8 M_\odot$ are in the far-UV or soft X-ray band, which are unobservable for most AGNs.

The observed ultraviolet (UV)/optical emission of AGNs is thought to be a thermal emission from the optically thick accretion flows (Shields, 1978; Malkan & Sargent, 1982; Sun & Malkan, 1989), while they are too cold to reproduce the observed power-law hard X-ray spectra of AGNs. The hard X-ray spectra of AGNs most likely originate from the inverse Compton process in which soft photons from the disks are scattered by the hot electrons in the coronas (Galeev et al., 1979; Haardt & Maraschi, 1991; Di Matteo, 1998). According to this disk-corona scenario, most gravitational energy is generated in the cold disk, while a fraction of it is carried into the corona likely by the magnetic loops in the disk (Di Matteo, 1998; Liu et al., 2002; Cao, 2009). Cao (2009) calculated the structure and spectrum of a geometrically thin accretion disk with a corona in AGNs, in which the corona is assumed to be powered by the reconnection of the magnetic loops originating from the cold accretion disk due to buoyancy

instability. It is found that both the hard X-ray bolometric correction factor $L_{\rm bol}/L_{\rm X,2-10keV}$ and the hard X-ray spectral index increase with the Eddington ratio, which are qualitatively consistent with the observations (e.g., Wang et al., 2004; Shemmer et al., 2006; Vasudevan & Fabian, 2007; Zhou & Zhao 2010; Fanali et al., 2013). This model was expanded in the general relativistic frame for a spinning Kerr black hole by You et al. (2012), in which the spectra of such a accretion disk-corona are recalculated taking into account general relativistic effect with the relativistic ray-tracing method.

As discussed above, the peaks of the spectra of the accretion disks surrounding massive black holes in AGNs are usually not observed (but also see Yuan et al., 2010, for the case of a relative small black hole in a narrow-line quasar). However, a portion of the soft photons originating from the disk undergoing Comptonization in the hot corona, and the scattered photons are dominantly in the hard X-ray band. This implies that the observed hard X-ray spectra (luminosity and spectral shape) contain the information of the incident spectra from the cold disk. It seems possible to constrain the values of black hole spin parameter a_* in AGNs with a general relativistic accretion disk corona model, as a variant of the continuum-fitting method, even if the spectral peaks of the accretion disks are not observed.

In this paper, we use the general relativistic model of an accretion disk-corona surrounding a spinning black hole to fit the observed multi-band spectra of AGNs with measured black hole masses. The black hole spinning parameter a_* are tentatively derived for a small sample of AGNs. We briefly summarize the accretion disk-corona model used for AGN spectral fitting in Section 2. The results and discussion are in Sections 3 and 4. Throughout this paper, a cosmology with $H_0 = 70{\rm km\,s^{-1}Mpc^{-1}}$, $\Omega_{\rm m} = 0.3$ and $\Omega_\Lambda = 0.7$ is adopted.

2 MODEL

In this work, we adopt the Kerr black hole accretion disk-corona model developed by You et al. (2012). All the general relativistic effects are properly considered in both the calculations of the structure and emergent spectra of the accretion disks. We briefly summarize the model in the next two sub-sections (see You et al., 2012, for the details).

2.1 Structure of an accretion disk with corona

In the accretion disk corona model, most gravitational energy of the gas is dissipated in the cold disk, and a portion of it is carried into the corona by the magnetic loops. The particles in the corona are heated by the re-connection of the loops in the corona (Di Matteo, 1998). The electrons in the corona are hot, and the observed hard X-ray spectra mostly originate from the inverse Compton process in which soft photons from the thermal radiation of the cold disk are scattered to high energy by the hot electrons (e.g., Galeev et al., 1979; Haardt & Maraschi, 1991; Svensson & Zdziarski, 1994).

The gravitational power of the gas generated in the cold accretion disk surrounding a spining black hole is

$$Q^+_{\rm dissi} = \frac{3GM\dot{M}}{8\pi R^3}\frac{L}{BC^{1/2}}, \tag{1}$$

where L, B, C are the general relativistic correction factors (Novikov & Thorne, 1973; Page & Thorne, 1974), and $\dot{M}$ is the mass accretion rate of the disk.

The fraction of the dissipated power transported to the corona can be estimated provided the strength of the magnetic field is known. The magnetic pressure of the disk is usually assumed to scale with the gas or/and radiation pressure of the disk depending on the different magnetic stresses adopted (Sakimoto & Coroniti, 1981; Stella & Rosner, 1984; Taam & Lin, 1984; Cao, 2009; Hirose et al., 2009). The detailed physics of the field generation is still quite unclear, though the different magnetic stressed are tested against the observations in AGNs in the previous works (Wang et al., 2004; Cao, 2009; You et al., 2012). For simplicity, the ratio f of the dissipated power in the corona to that in the disk is taken as a parameter in our model calculations,

$$f = \frac{Q^+_{\rm cor}}{Q^+_{\rm dissi}}, \tag{2}$$

which will be determined by the comparison with the observed spectra.

A portion of the soft photons from the disk undergo inverse Comptonization to high energy in the corona, which correspondingly cools the electrons in the corona. About half of the scattered photons are intercepted by the disk, some of which are reflected and the rest heats the disk and re-radiate as blackbody radiation (Zdziarski et al., 1999). Therefore the energy equation for the cold disk is

$$Q^{+}_{\rm dissi} - Q^{+}_{\rm cor} + \frac{1}{2}(1-\varepsilon)Q^{+}_{\rm cor} = \frac{4\sigma T_{\rm d}^4}{3\tau} = \sigma T_{\rm s}^4, \tag{3}$$

where the reflection albedo $\varepsilon = 0.15$ is adopted in all our calculations (Zdziarski et al., 1999), $\tau = \tau_{\rm es} + \tau_{\rm ff}$ is the optical depth in the vertical direction of the disk, and $T_{\rm d}$ and $T_{\rm s}$ are the temperature in the mid-plane of the disk and the temperature of the gas at the disk surface respectively.

2.2 Emergent spectrum of the accretion disk with corona

It is well known that most of the radiation of the disk comes from the inner region of the disk (Shakura & Sunyaev, 1973). The spectrum of an accretion disk-corona for a spinning black hole is influenced by the relativistic effects, i.e., the frame dragging, gravitational redshift, and photon trajectory bending, due to the strong gravity field of the black hole (Zhang et al., 1985; Laor & Netzer, 1989; Laor, 1991; Li et al., 2005, 2009; You et al., 2012), especially for the emission from the region near the black hole. The ray-tracing method is widely adopted in this kind of spectral calculations (Laor & Netzer, 1989; Laor, 1991; Zhang et al., 1997; Li et al., 2005; You et al., 2012). Considering the complexity of the radiation transfer of Comptonized photons in the geometrically thick corona, You et al. (2012) calculated the emergent Comptonized spectrum from the corona by dividing layers in the corona with the ray-tracing method. In this work, we follow the same routine of You et al. (2012) to calculate the spectrum of an accretion disk-corona for a rotating black hole, in which all the general relativistic effects are taken into account (see Section 3.4 in You et al., 2012, for the details)

The radiation from geometrically thin, optically thick accretion disk is anisotropic, and the specific intensity of the disk emission, $I_\mu \propto (1+2\mu)$, in the co-moving frame of the disk, where $\mu = \cos\theta$ (θ is the angle between the line of sight and the normal of the disk Chandrasekhar, 1960; Sunyaev & Titarchuk, 1985; Liu & Zhang, 2011).

UV/soft X-ray photons are emitted from the inner region of the accretion disk, where a hot plasma layer is present above the disk surface caused by the illumination of the external hard X-ray emission from the corona. The electron scattering opacity dominates over absorption in this hot layer, and the emergent spectrum of the disk departures from the black body emission due to radiative transfer. Hubeny et al. (2001) calculated the vertical structure and emergent spectra of the disks with a hot plasma layer by including a self-consistent treatment of Compton scattering. Chiang (2002) found that the derived emergent spectrum could be well reproduced by blackbody emission with a higher color temperature, $T_{\rm rad} = f_{\rm col} T_{\rm d}$. The empirical color correction factor $f_{\rm col}$ is given by

$$f_{\rm col}(T_{\rm d}) = f_\infty - \frac{(f_\infty - 1)[1+\exp(-\nu_{\rm b}/\Delta\nu)]}{1+\exp[(\nu_{\rm p}-\nu_{\rm b})/\Delta\nu]} \tag{4}$$

where $\nu_{\rm p} \equiv 2.82 k_{\rm B} T_{\rm d}/h$, $f_\infty = 2.3$ and $\nu_{\rm b} = \Delta\nu = 5\times10^{15}$Hz. The local spectrum emitted from the disk can be calculated with

$$F_\nu \propto \frac{1}{f_{\rm col}^4} \pi I_\nu (f_{\rm col} T_{\rm d}), \tag{5}$$

where I_ν is the local blackbody emission.

As described in Section 2.1, the structure of the accretion disk-corona can be calculated when the values of the black hole mass M, the dimensionless spin a_*, the mass accretion rate $\dot{m}$, and the ratio f of the dissipated power in the corona to that in the disk, are specified. With the derived structure of the accretion disk, we use the ray tracing method to calculate the emergent spectrum of the disk corona system observed in infinity at a viewing angle θ. We plot the representive emergent spectra with different

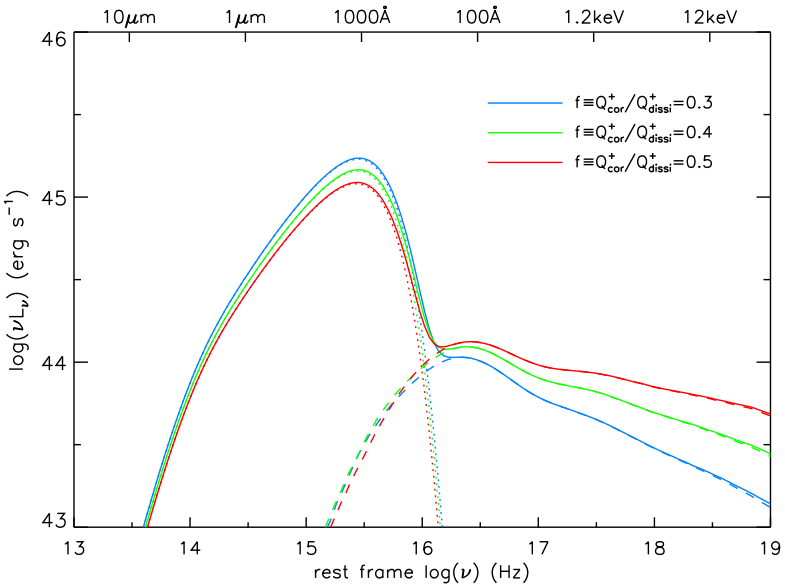

Fig. 1 The representtive spectra of the disk-corona model with different values of the ratio f of the dissipated power in the corona to that in the disk. The dotted lines represent the spectra of the disk blackbody radiation, while the dashed lines represent the Compton radiation from the corona. The synchrotron and bremsstrahlung radiation which dominate in radio bands are not plotted. It is found that the hard X-ray spectra become harder with the ratio f.

values of the ratio f in Fig. 1 to show the effect of f on the overall shape of the spectra. At a given radius, both the energy dissipated in the disk and the disk temperature decrease with energy ratio f according to Eq. (2). Therefore, the specific intensity of the soft photons from the disk will also decrease with the ratio f. In this case, the electron temperature will increase with f, since the cooling of the corona is dominated by the inverse Compton scattering of the soft photons from the disk by the hot electrons in the corona (Cao, 2009; You et al., 2012). This means that the resulting spectra in the hard X-ray band become much harder and brighter with the increase in the ratio f, given that more soft photons from the disk will be Compton scattered to higher energy by the hot electrons in the corona (see Fig. 1).

3 RESULTS

Using the accretion disk model described in Section 2, we fit the observed multi-band spectral energy distributions (SEDs) of five quasars which exhibit obvious feature of so-called "Big Blue Bump" (BBB) with measured black hole masses and good X-ray measurements. The peak of BBB at $\sim 10^{15}-10^{16}$ Hz and a power-law hard X-ray spectrum are the typical features of the spectrum of an accretion disk with corona (e.g., Cao, 2009; You et al., 2012). As discussed in Section 1, the peaks of the BBBs are beyond the waveband coverage of the instruments for most AGNs due to their massive black holes. However, the left tail of the BBBs can be observed in infared/optical/UV wavebands, which provide useful information of the BBBs (e.g., Calderone et al., 2013). The SED data of five quasars in this work is taken from Shang et al. (2011) and summarized in Tables 1 and 2.

The black hole masses M of these five quasars are given in Tang et al. (2012), which are estimated with the broad-line width and the scaling relationships (Vestergaard & Peterson, 2006; Vestergaard & Osmer, 2009). The infrared emission from these quasars may probably be dominated by the radiation from the dust tori, while the origin of the soft X-ray excess observed in AGNs is still controversial (see,

Table 1 The SED data in optical/UV wavebands

Object	Other name	R.A.(J2000)	Decl.(J2000)	z	$E(B-V)^{\rm a}$	$\lambda L_\lambda(3000\mathring{A})^{\rm b}$	SampleID
PG 1322+659		13:23:49.54	+65:41:48.0	0.1684	0.019	44.61	RQ
PG 1115+407		11:18:30.20	+40:25:53.0	0.1541	0.016	46.53	RQ
4C 10.06	PKS 0214+10	02:17:07.66	+11:04:10.1	0.4075	0.109	45.54	RL
4C 39.25	B2 0923+39	09:27:03.01	+39:02:20.9	0.6946	0.014	45.70	RL
OS 562		16:38:13.45	+57:20:24.0	0.7506	0.013	43.51	RL

Notes: † (a) From NED(http://nedwww.ipac.caltech.edu/) based on Schlegel et al. (1998). (b) the rest-frame luminosity at 3000Å.

Table 2 The X-Ray Spectral data

Object	E1	E2	E3	$f_\nu = f_0 E^\alpha$				Reference
				f_0	α	f_0	α	
(1)	(2)	(3)	(4)	(5)	(6)	(7)	(8)	(9)
PG 1322+659	0.3	1.62	10.0	6.51E-4	$-2.01^{+0.24}_{-0.11}$	4.36E-4	$-1.18^{+0.14}_{-0.11}$	X,Po04
PG 1115+407	0.3	2.04	10.0	6.48E-4	$-1.85^{+0.06}_{-0.02}$	4.05E-4	$-1.19^{+0.10}_{-0.10}$	X,Po04
4C 10.06	0.1		2.4	9.08E-4	$-1.13^{+0.52}_{-0.56}$			R,Br97
4C 39.25	0.1		2.4	5.83E-4	$-1.25^{+0.06}_{-0.06}$			R,Br97
OS 562	0.1		2.4	1.36E-4	$-1.38^{+0.04}_{-0.04}$			R,Br97

Notes: †For the sources PG 1322+659 and PG 1115+407, their X-ray spectra are fitted by a broken power law model in the ranges of $E1-E2$ and $E2-E3$ (keV) in the observer's frame. The remainders are fitted by a single power law model between $E1$ and $E3$. The columns (5) and (7) are the flux densities at 1 keV in units of mJy ($10^{-26}{\rm erg\,s^{-1}cm^{-2}Hz^{-1}}$); E in keV.

References: R,C,X indicate data sources, corresponding to ROSAT, Chandra, and XMM, respectively. Br97: Brinkmann et al. (1997); Po04: Porquet et al. (2004)

Table 3 The fitting parameters of the sources

Object	log$M$	f	a_*	$\dot{m}$	θ	T_e(keV)	χ^2/dof
PG 1322+659	8.29	$0.47^{+0.10}_{-0.12}$	$-0.94^{+0.14}_{-0.06}$	$0.388^{+0.019}_{-0.020}$	$25.7^{+3.5}_{-4.7}$	265.3	2.8/9
PG 1115+407	8.18	$0.41^{+0.06}_{-0.03}$	$-0.55^{+0.15}_{-0.15}$	$0.420^{+0.020}_{-0.005}$	$10.0^{+7.3}_{-3.1}$	241.2	4.3/5
4C 10.06	9.00	$0.60^{+0.15}_{-0.10}$	$0.7^{+0.05}_{-0.05}$	$0.415^{+0.020}_{-0.017}$	$39.4^{+2.2}_{-2.0}$	194.7	4.9/7
4C 39.25	9.33	$0.47^{+0.03}_{-0.02}$	$0.998^{+0.000}_{-0.004}$	$0.344^{+0.008}_{-0.011}$	$42.5^{+0.9}_{-1.4}$	158.3	11.5/11
OS 562	8.92	0.33	$0.96^{+0.03}_{-0.04}$	$0.505^{+0.027}_{-0.020}$	$13.0^{+7.2}_{-9.6}$	142.5	4.3/7

Notes: The black hole mass M is taken from Tang et al. (2012). T_e is the maximum value of the electron temperature of the corona, which is calculated with the best-fitting values of free parameters a_* and $\dot{m}$.

e.g., Done et al., 2012, and the references therein). Therefore, the infrared and soft X-ray spectral data are not used in our model fitting on the SEDs.

We use the general relativistic accretion disk corona model to fit the observed optical/UV spectra and the hard X-ray continuum spectra in $2-10$ keV. There are four free parameters in our model calculations, i.e., the mass accretion rate $\dot{m}$, the spin parameter a_*, the power fraction f dissipated in the corona, and the viewing angle θ with respect to disk axis. In the spectral fitting, we find that the fraction f is mainly determined by the X-ray spectral index, which is almost independent of the values of other parameters. For the broad-line type I quasars, the values of the inclination angle are tuned in the range of $\theta \lesssim 45^\circ$.

We plot the spectral fitting results of the five quasars in Figures 2-6. In the optical/UV wavebands, the data points (marked as blue filled circles) which are used in our spectral fitting are extracted from the observed SED in the line-free continuum windows in order to avoid the contamination by emission lines, as done in Zheng et al. (1997) and Vanden Berk et al. (2001).

In this work, the measured hard X-ray luminosity and the spectral index are used for our spectral fitting. In the spectral fitting, the errors of the fitting in the hard X-ray band (both the luminosity and

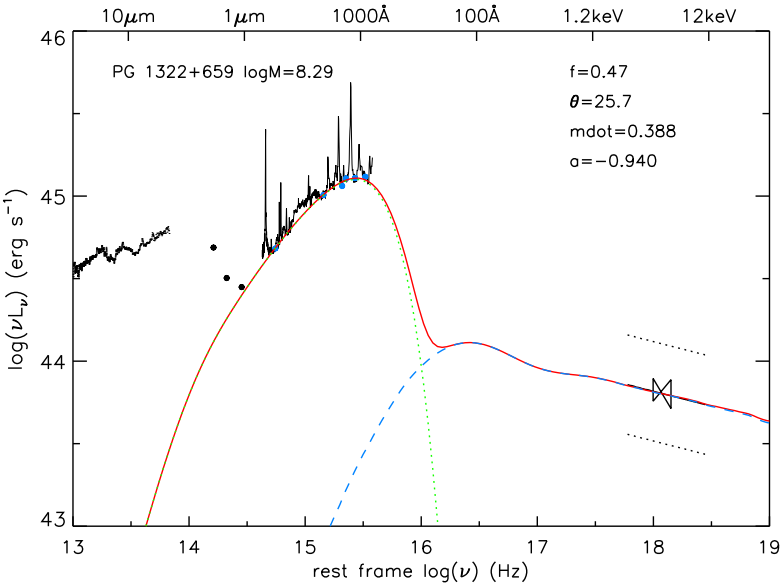

Fig. 2 The spectral fitting results for PG 1322+659. The radio and near infrared data are not used in our accretion disk corona spectral fittings. The photometric points marked as blue filled circles are used for fitting. The solid black line represents the power law X-ray spectrum in $2-10$ keV. The red line represents the best fitting result with the black hole mass $\log M = 8.29$. The green dotted line represents the spectrum of the cold disk, while the blue dashed line is for the Compton radiation. The synchrotron and bremsstrahlung radiation which dominate in radio bands are not plotted.

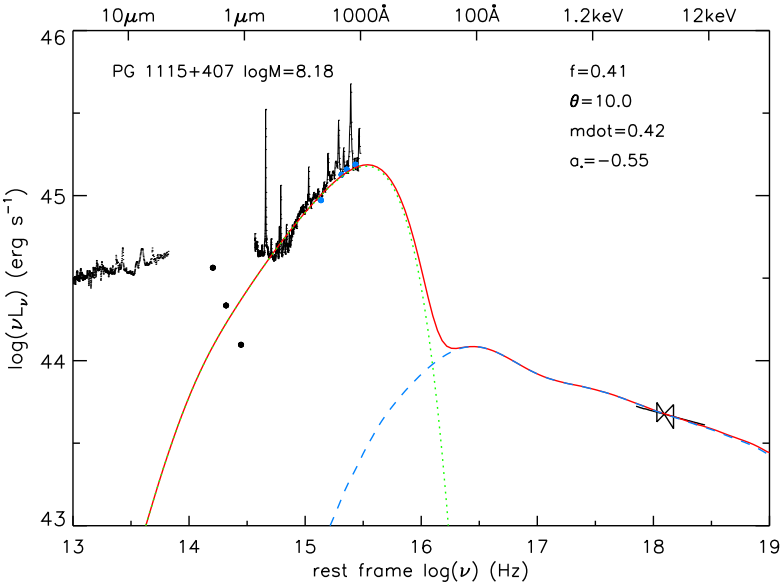

Fig. 3 The best fitting result for PG 1115+407.

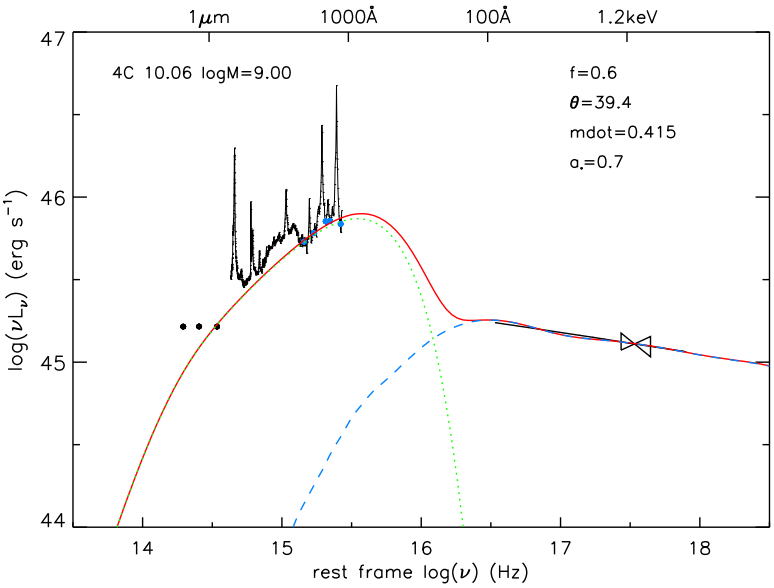

Fig. 4 The same as Figure 2, but for 4C 10.06.

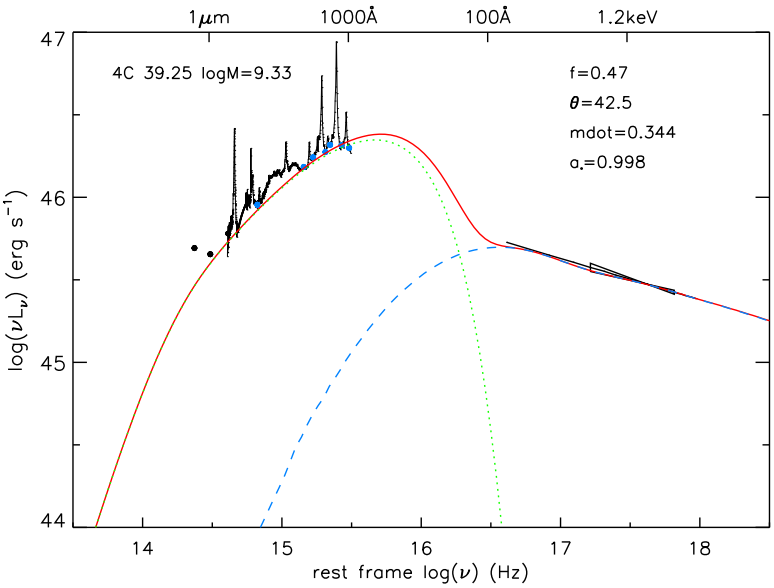

Fig. 5 The same as Figure 2, but for 4C 39.25.

spectral index) are minimized by tuning the model parameters, meanwhile the observed optical/UV spectrum is taken as upper limits.

The best-fitting results of the disk corona parameters are listed in Table 3. The error of the parameter f is determined according to the error of the hard X-ray spectral index α in Table 2, given that f strongly

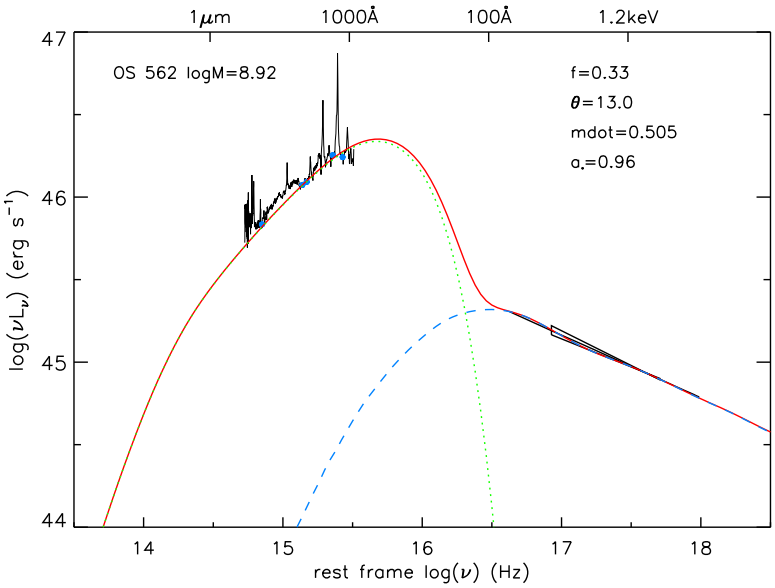

Fig. 6 The same as Figure 2, but for OS 562.

depends on α. The fitting error χ^2 is calculated in the parameter plane, and the distributions of the error contour for the spin a_*, the mass accretion rate $\dot{m}$ and the inclination angle θ are plotted in Fig. 7. The uncertainties on the three parameters correspond to 90% confidence level. . The 2D confidence contours of a_* and $\dot{m}$ for PG 1322+659 with the measured black hole mass M and fraction f are plotted in Fig. 8. We find that, the value of black hole spin parameter is constrained in a narrow range $-1.0 < a_* < -0.8$ with best-fitting value $a_* = -0.94$. The best-fitting accretion rate $\dot{m} \simeq 0.4$, and the inclination angle of the disk $\theta \simeq 25°$. We know that uncertainties of the black hole spin constraints are closely related to the errors of the black hole mass estimates. In Fig. 9, we plot the fitting results for PG 1322+659 with the different values of M reported in the literature, and find that the constraints on the black hole spin parameter a_* are sensitive to the black hole mass estimate (see Table 4). Within the uncertainties of a factor of four on the mass measurements (Vestergaard & Peterson, 2006), using single epoch reverberation mapping method, from $2 \times 10^8 M_\odot$ to $8 \times 10^8 M_\odot$ with the step of $10^8 M_\odot$, the best-fitting values of black hole spin can vary from -0.94 to 0.998 (see Fig. 10). In Fig. 11, we plot the fitting results for PG 1322+659 with a small shift $\Delta \log L_{\rm X}$ on the observed X-ray luminosity to assess how the black hole spin a_* is affected by X-ray variability (see Table 4).

We fit the emission line properties of PG 1322+659 by subtracting the best spectral fitting continuum in Fig. 12, to compare with the typical broad line region spectrum. The derived EW and FWHM for Mg II, Hβ, and Hγ are consistent with those of the typical BLR spectrum given in Shen et al. (2011). In Fig. 13, we plot the relative disk thickness $H_{\rm d}/R$ varying with the mass accretion rate $\dot{m}$. It is found that the thin disk approximation $H_{\rm d}/R \lesssim 0.1$ can be achieved even if $\dot{m} > 0.3$. Note that when the mass accretion rate $\dot{m}$ is as high as ~ 0.5, $H_{\rm d}/R$ is only slightly larger than 0.1 for a typical value of $f \sim 0.5$.

4 DISCUSSION

The main features of quasar SED with a big blue bump in optical/UV wavebands and a power-law hard X-ray continuum spectrum can be reproduced by the accretion disk corona scenario (Galeev et al., 1979; Qiao & Liu 2015). There are various models which are developed in the exploring the radiation from the

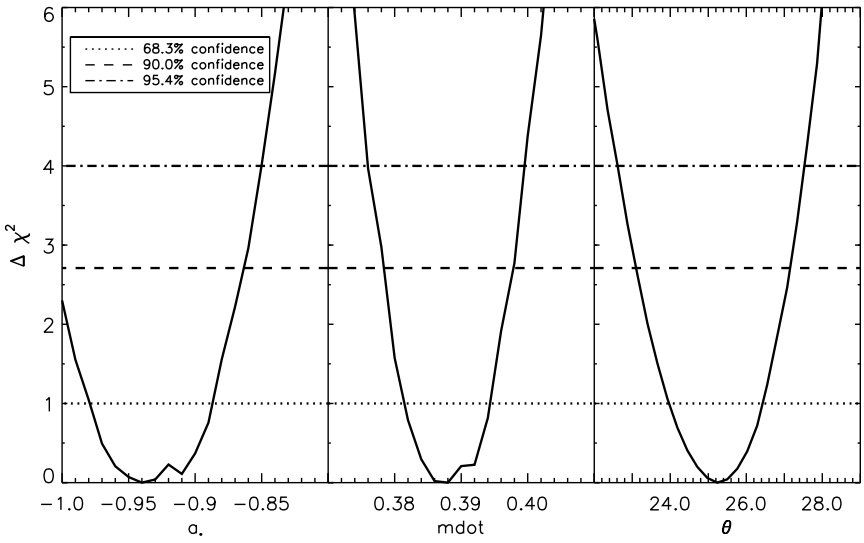

Fig. 7 Error contour for the spin parameter a_*, the mass accretion rate $\dot{m}$ and the inclination angle θ. The three horizontal lines, from bottom to top, are corresponding to the 68.3%, 90.0% and 95.4% confidence, respectively.

Table 4 The spectral fitting results of PG 1322+659

ID	log$M$	f	a_*	$\dot{m}$	θ
1	8.29	0.47	-0.94	0.388	25.7
2	8.36	0.47	-0.75	0.316	29.8
3	8.16	0.47	-0.94	0.520	0.0
4	8.59	0.47	0.90	0.06	30.0
5	8.89	0.47	0.94	0.03	43.0
6	8.29	0.47	-0.7	0.5	37.0
7	8.29	0.47	-1.0	0.3	0.0

Notes: The spectral fitting results with different black hole masses in the literature (ID 2-5) and the variation of the X-ray luminosity (ID 6,7). The fitting results are plotted in Fig. 9 and 11 respectively.

accretion disk and corona. For instance, KERRBB is a relativistic multi-temperature blackbody model for the thin accretion disk around a Kerr black hole, which is usually used to fit the disk emission from disk-dominated X-ray binaries and quasars (Li et al., 2005), while SIMPL is a Comptonization model for modeling the power-law hard X-ray spectra of X-ray binaries and AGNs (Steiner et al., 2009b). The convolution between KERRBB and SIMPL in XSPEC (Arnaud, 1996) could simulate the broad band SEDs of quasars, namely, the optical BBB and power-law X-ray spectra, for the purpose of our paper here. In the resulting spectra of SIMPL*KERRBB, the hard X-ray power-law index depends on the parameter Γ, while the flux is determined by the parameters $f_{\rm SC}$ which is the fraction of the soft photons from the disk being scattered to high energy (see Fig. 1 in Steiner et al., 2009b). As an alternative Comptonization model, a general relativistic model for an accretion disk corona surrounding a Kerr black hole was developed by You et al. (2012), in which the energy fraction dissipated into the corona was assumed in order to solve the pattern of the disk corona system. The emergent spectrum of the disk corona observed at infinity can be calculated when the values of the disk parameters are specified.

In this work, we try to fit the observed SEDs of quasars with the general relativistic accretion disk corona model, in which the values of the disk parameters for five quasars, especially the black hole spin parameter a_*, are derived. The black hole masses of these quasars are estimated with single epoch reverberation mapping method (see Tang et al., 2012, for the details).

The red tail of the BBB in optical wavebands is mostly emitted from the outer region of the accretion disk, which can be used to constrain the mass accretion rate $\dot{m}$ almost independent of the black hole spin parameter a_* if the black hole mass M and the inclination angle θ are known (see Davis & Laor, 2011). In our accretion disk corona model, the mass accretion rate $\dot{m}$ can be inferred similar to their work. The peaks of the BBBs in most quasars are in the far-UV/soft X-ray wavebands, which are usually unobserved. This is sensitive to the black hole spin a_*, which is the main obstacle for measuring the spin parameters a_* of massive black holes with the spectral fitting method. In the accretion disk corona model considered in this work, the photons emitted from the disk, including the unobserved far-UV/soft X-ray photons are inverse Compton scattered in the hot corona, and the hard X-ray spectra (luminosity and spectral shape) contain the information of the incident spectra from the cold disk.

The fraction f of the power dissipated in the corona to the total power is a key parameter in the accretion disk-corona model. The detailed physical processes for the energy transported from the disk to the corona were explored by many different authors (e.g., Di Matteo, 1998; Meyer et al., 2000; Liu et al., 2002; Wang et al., 2004; Cao, 2009). It is found that both the hard X-ray spectral index and the hard X-ray bolometric correction factor $L_{\rm bol}/L_{\rm X,2-10keV}$ are correlated with the Eddington ratio (e.g., Wang et al., 2004; Shemmer et al., 2006; Vasudevan & Fabian, 2007; Zhou & Zhao 2010; Fanali et al., 2013), which can be reproduced roughly by the accretion disk corona model on the assumption that the corona is heated by the reconnection of the magnetic fields generated by buoyancy instability in the cold accretion disk (Cao, 2009). However, the precise value of f is still undetermined in the theoretical model calculations. In this work, we adopt the fraction f as a free parameter in the spectral fittings.

In the spectral fitting of a quasar SED with measured black hole mass, the value of f is dominantly determined by the hard X-ray photon index Γ, which is almost insensitive to all other model parameters (Cao, 2009; You et al., 2012). With the derived value of f from Γ, the mass accretion rate $\dot{m}$ and the inclination angle θ are constrained with the luminosity and spectral shape in optical waveband (the red tail of the BBB). These two parameters are almost independent of the black hole spin parameter a_*, because the emission in this waveband is dominantly from the outer region of the disk (Davis & Laor, 2011) . Finally, the black hole spin parameter a_* is constrained mainly with the observed hard X-ray luminosity.

In Figures 2-6, we plot the fitting results of five quasars. The values of black hole spin parameter a_* are well constrained with small uncertainties, which are in the range of ~ -0.94 to 0.998 (see Table 3). The estimated accretion rate is moderate, approximately 0.4 except OS 562 with $\dot{m} \simeq 0.5$, and these quasars are possibly viewed with small inclination angles $< 45^\circ$, which support the classification of the sources as type 1 quasars. The fractions f of the power radiated in the corona to the total dissipated power in the disk are $\sim 0.3 - 0.6$ (see Table 3).

In the spectral fitting on the SEDs of these sources in this work, the electron temperatures of the coronas are in the range of $100 - 300$ keV, which are roughly consistent with the previous works (e.g., Zdziarski et al., 1996; Liu et al., 2002). The maximal temperatures of the electrons in the coronas for the sources are listed in Table 3. The corresponding cutoff energy of the X-ray spectra is around several hundred keV (see You et al., 2012). No direct observations in this energy band are available for these five sources. The cutoff energy in the power law X-ray spectra is observed only in a small fraction of AGNs, which is typically in the range of $30 - 300$ keV (Molina et al., 2013). This is consistent with our results.

We plot the distribution of the fitting error $\Delta\chi^2$ for the spin a_*, the mass accretion rate $\dot{m}$ and the inclination angle θ in Fig. 7, in which the uncertainties of the fitted parameters are given by 90% confidence levels. We also plot 2D confidence contours in Fig. 8, and find that the black hole spin a_* is indeed well constrained at fairly good accuracy if the black hole mass is accurately measured.

The observed hard X-ray spectra may be affected by the reflection components (Gou et al., 2011, 2014). However, there are observational evidences that the reflection components are absent in many

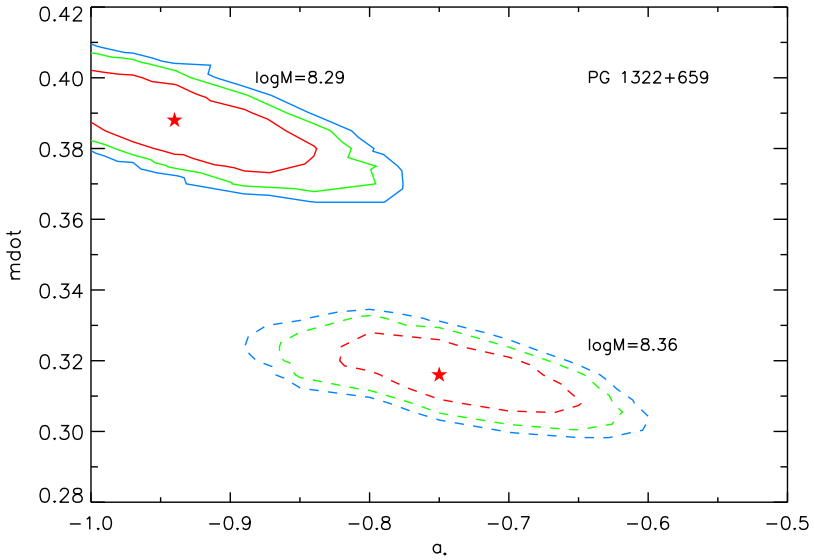

Fig. 8 The confidence contours (red:68.3%, green:90.0%, blue:95.4%) for the black hole spin a_* and the accretion rate $\dot{m}$ of PG 1322+659, for two black hole masses $\log M = 8.36$ and$\log M = 8.29$. For $\log M = 8.16$, the spectrum is not fitted well. The star indicates the position of the best fit. The fraction $f = 0.47$ is adopted.

bright quasars (high luminosities) (Nandra et al., 1997; Page et al., 2005; Gilli et al., 2007). The *XMM-Newton* observations of a sample of high redshift quasars show that the hard X-ray spectra (> 10 keV in the rest frame of the sources) can be well fitted for each source by a simple power law, and no Compton reflection humps are present (Page et al., 2005). The five sources in this work are all luminous quasars with $\dot{m} \gtrsim 0.3$, and therefore we believe that their hard X-ray continuum spectra may probably not be contaminated by the reflection components. Further X-ray observations in high energy with/without Compton reflection hump for these sources may help resolve this issue.

Another uncertainty of the black hole spin constraints is caused by the errors of the black hole mass estimates, because the constraints on the spin parameter a_* is sensitive to the black hole mass (see Table 4). The black hole spin of quasar SDSS J094533.99+100950.1 is derived by fitting its multi-band (IR/optical/UV) continuum spectrum. The black hole spin a_* varies from -1.0 to 0.998 if the black hole mass is taken as a free parameter, which means that the black hole mass is crucial in constraining the black hole spin a_* (Czerny et al., 2011). In order to evaluate how the constraint on the spin parameter a_* is affected by the black hole mass, we re-fit the SED of PG 1322+659 with different values of black hole mass given in different works (see Table 4). For the black hole mass $\log M = 8.36$ estimated with C IV line (Vestergaard & Peterson, 2006), the best fitting of black-hole spin appears as $a_* = -0.75$, while $a_* = -0.94$ if $\log M = 8.29$ is adopted. For the black hole mass $\log M = 8.16$ estimated by Kawakatu et al. (2007), no satisfactory spectral fitting is available. In most previous works, the uncertainty of the black hole mass estimates with single epoch reverberation mapping approach is within a factor of four (e.g., Wu et al., 2004; Peterson et al., 2004; Vestergaard & Peterson, 2006). Increasing the mass $\log M = 8.29$ by a factor of two and four, i.e., $\log M = 8.59, 8.89$, we find that the black hole spin parameters are constrained as $a_* = 0.9, 0.94$ respectively (see Fig. 9). With typical accuracy of the black hole mass measurements, the best fitted black hole spins are in a large range from -0.94 to 0.998 (see Fig. 10), which indicates that no tight constraint on the black hole spin is achieved with the uncertainty of a factor of four in mass estimates. However, it is not unique. Actually this issue is already discovered

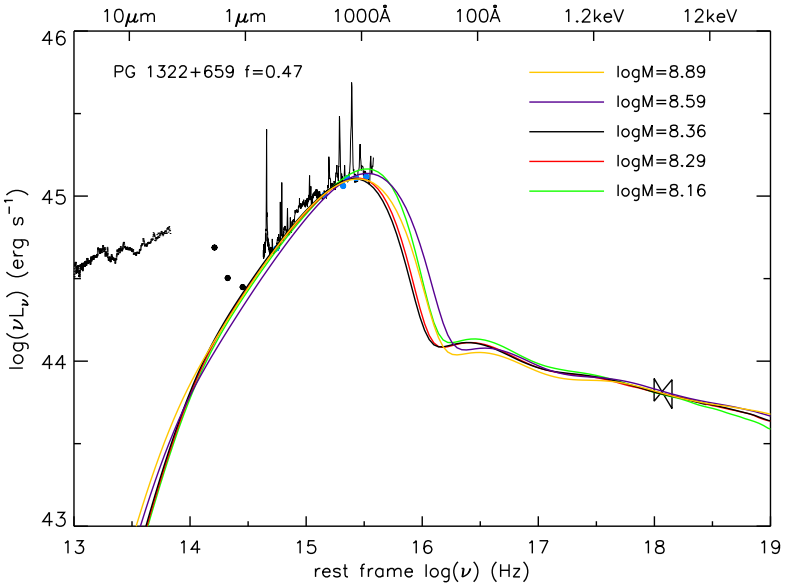

Fig. 9 The same as Fig. 2, but with different black hole masses reported in the literature: $\log M = 8.36$ (Vestergaard & Peterson, 2006); $\log M = 8.16$ (Kawakatu et al., 2007) as well as increased by a factor of two and four:$\log M = 8.59$, $\log M = 8.89$. The fitting results are, yellow line: $a_* = 0.94$, $\dot{m} = 0.03$, $\theta = 43.0$; purple line: $a_* = 0.90$, $\dot{m} = 0.066$, $\theta = 30.0$; black line: $a_* = -0.75$, $\dot{m} = 0.316$, $\theta = 29.8$; red line: $a_* = -0.94$, $\dot{m} = 0.388$, $\theta = 25.7$; green line: $a_* = -0.94$, $\dot{m} = 0.52$, $\theta = 0.0$.

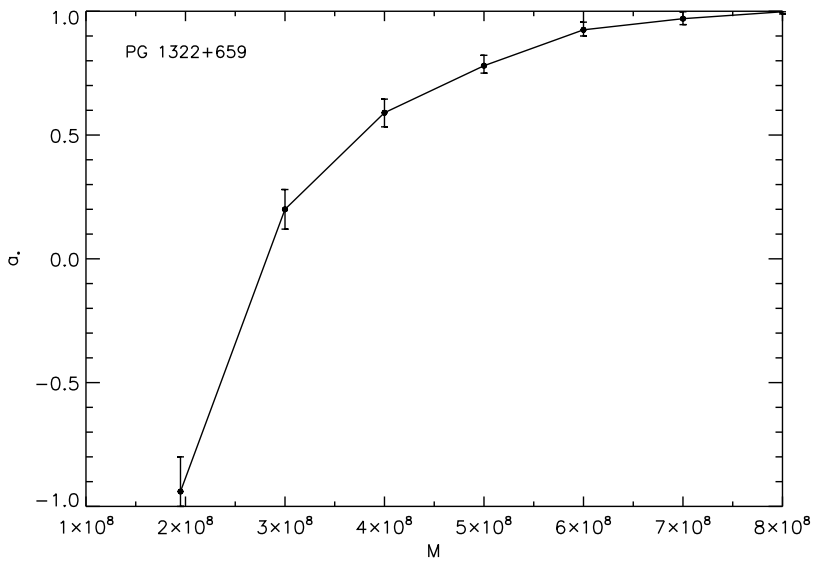

Fig. 10 The best-fitting values of black hole spin for the different black hole masses from $2 \times 10^8 M_\odot$ to $8 \times 10^8 M_\odot$, with the step of $10^8 M_\odot$.

by previous works when the continuum-fitting method is applied to both AGNs and X-ray binaries. For instance, as for AGNs, the best-fitting values of the spin a for different black hole masses and the inclination angles can be found in Fig 5 of Done et al. (2013), which showed that the spin could vary from -1 to 1 if the mass is in a large range; as for X-ray binaries, even the system parameters of LMC X-3 are fairly well determined, the spin can spread over a large range with different combinations of the blacho hole mass and inclination angle (see Table 2 of Kubota et al., 2010). The improved estimate of the spin of LMC X-3 $a_* = 0.25$ (Steiner et al., 2014), with the dynamical parameters to date (Orosz et al., 2014). Although the spin covers almost all the possible range for the spin parameter due to large errors of the black hole mass, fitting the disk-corona model to the optical/UV and X-ray SED in our paper is meriting exploration.

The main uncertainty of traditional reverberation mapping analysis originates from the virial coefficient or normalizing factor. Recently, Pancoast et al. (2011) proposed a method to analyze reverberation mapping data, with which the geometry and kinematics of the BLR can be well constrained by modeling the continuum light curve and broad line profiles directly with the velocity resolved broad line data. This allows to make a measurement of the black hole mass that does not depend on the virial coefficient (Pancoast et al., 2011, 2012). The accuracy of the black hole mass estimates with this method has been significantly improved (Barth et al., 2011; Pancoast et al., 2012; Li et al., 2013). The preliminary results show that five black hole masses have been measured at an uncertainty of $\sim 0.2 - 0.4$ dex depending upon data quality with this method (Pancoast et al., 2014). We search the literature, and find that the X-ray spectral data are available only for the two sources. Unfortunately, the X-ray photon spectral index $\Gamma < 2$ for these two sources, which are unsuitable for our present investigation. The black hole spins can be well constrained with the method in this work, when a variety of black hole masses are measured at an uncertainty of ~ 0.2 dex with the velocity resolved reverberation mapping method in the near future.

In our model calculations, the hard X-ray emission of these quasars is assumed to originate predominantly from the corona above the disk, which is true for radio quiet sources. However, it should be cautious for radio loud quasars, of which the observed hard X-ray emission may be contaminated by the beamed jet emission (e.g., Chen et al., 2012). We find that OS 562 is a Flat Spectrum Radio Quasar (FSRQ), which is also characterized as low-spectral peaked source with the synchrotron peak frequency $\nu_{\rm p} < 10^{14}$Hz (Lister et al., 2009). The Very Long Baseline Array (VLBA) observations indicate that this source is observed with a small inclination angle with respect to the jet axis (Lister, 2001), which is consistent with the viewing angle $\theta = 13^\circ$ derived in our spectral fitting (see Table 3). Donato et al. (2001) analyzed the X-ray spectral of 268 blazars including BL Lacs and FSRQs, and found that the X-ray spectra of FSRQs are always hard, i.e., the average X-ray spectral index $\alpha \simeq -0.76$ ($\Gamma \simeq 1.76$). The X-ray spectral index of OS 562 is -1.38, much softer than a typical FSRQ, which may imply that the X-ray emission is predominantly from the corona. This is the case also for the other two radio quasars. The radio core dominance R (defined as $R = L_{\rm core}/L_{\rm ext}$) is usually taken as a radio orientation indicator (Ghisellini et al., 1993; Wills & Brotherton, 1995). The radio core dominance parameters of the other two radio loud quasars in this work are, $\log R = -0.658$ (4C 10.06) and -2.22 (4C 39.25) (Runnoe et al., 2013), which imply that the jets are inclined at large angles with respect to the line of sight. This is consistent with our fitting results of $\theta \simeq 40^\circ$ for these two sources. The beaming effects for the jets viewed at such large angles are always unimportant (e.g., Wu et al., 2013). This strengthens the conclusion that the beamed X-ray emission from the jets can be neglected compared with that from the coronas in these two sources.

Although there are no additional information of X-ray variability for 4C 10.06 and OS 562, some previous observations indicated that the other three sources have low X-ray variability, $\Delta \log L_{\rm X} = 0.03, 0.1$ for PG 1322+659 and PG 1115+407 (Grupe et al., 2001), $10\% \sim 30\%$ variation for a sample of flat-spectrum radio quasars including 4C 39.25. In Fig. 11, we show that the constraint on the black hole spin a_* is affected by the X-ray variability. It is found that the spin parameter becomes $a_* = -1$ for $\Delta \log L_{\rm X} = -0.1$, while $a_* = -0.7$ for $\Delta \log L_{\rm X} = 0.1$. This implies that the sources with violent variability are not suitable for present investigation on black hole spin. Our model is applicable for steady accretion disk corona systems. For those slightly variable sources, the mean observed continuum spectrum can still be used to constrain the black hole spin parameters.

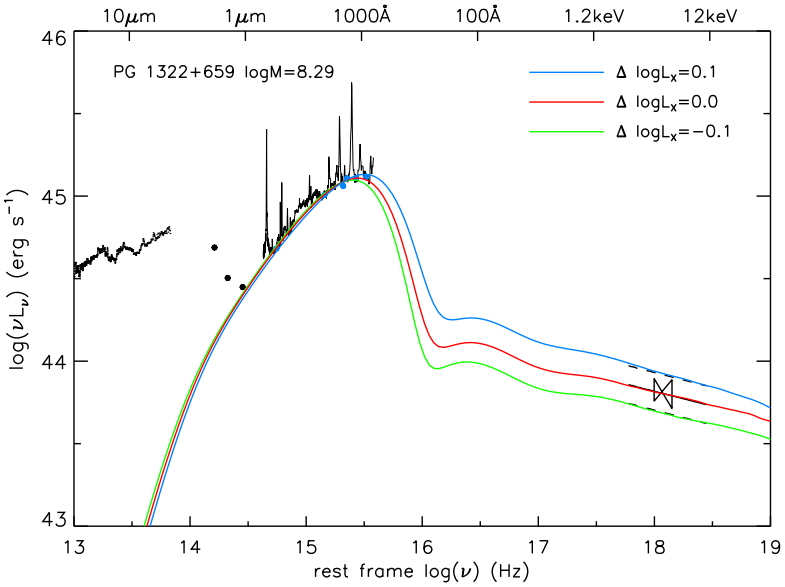

Fig. 11 The same as Fig. 2, but with a small shift $\Delta \mathrm{logL_X} = \pm 0.1$ on the observed X-ray luminosity (dashed lines) to assess how the black hole spin a_* is affected by X-ray variability. The parameters $\mathrm{logM} = 8.29$ and $f = 0.47$ are adopted. The fitting results are, blue line: $a_* = -0.7$, $\dot{m} = 0.5$, $\theta = 37.0$; red line: $a_* = -0.94$, $\dot{m} = 0.388$, $\theta = 25.7$; green line: $a_* = -1.0$, $\dot{m} = 0.3$, $\theta = 0.0$.

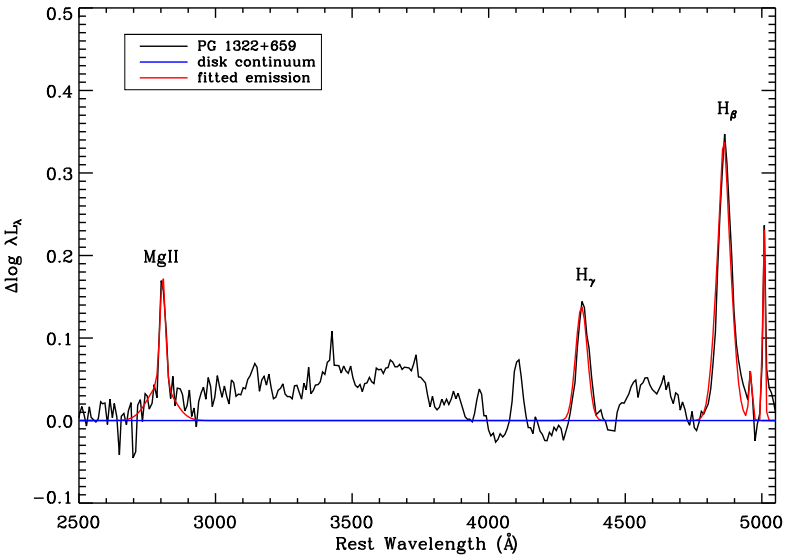

Fig. 12 The residual emission line spectrum for PG 1322+659 marked as black line, with the best fit continuum from the Fig. 2 being subtracted. The fitted emission lines of Mg II,H$\gamma$and H$\beta$are marked with red lines.

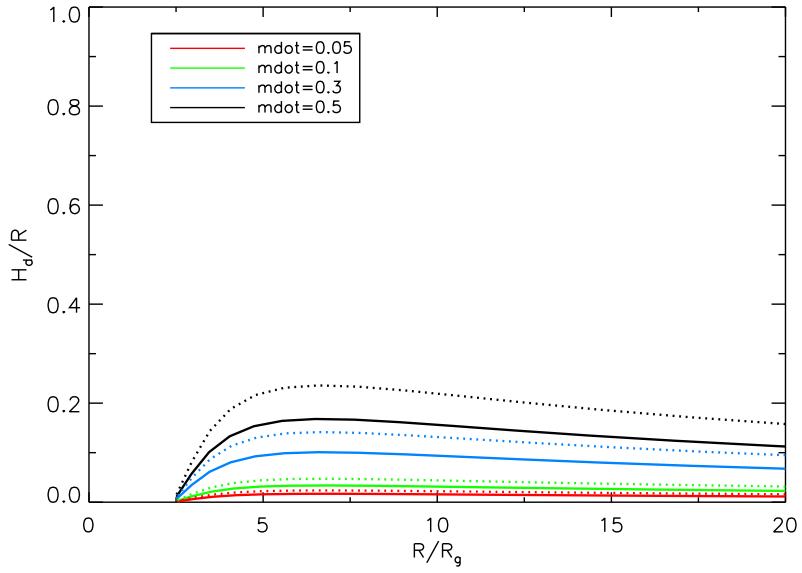

Fig. 13 The relative disk thickness $H_{\rm d}/R$ as functions of radius with different accretion rates $\dot{m}$ for a given black hole mass $M = 10^8 M_{\odot}$ and spin $a_* = 0.9$. The solid lines represent the results for disks with coronas, while the dotted lines are for bare accretion disks without corona. The colored lines represent the model calculations with different values of accretion rates.

Although the soft X-ray spectral data are not used in our model fitting on the SEDs, given the origin of the soft X-ray excess observed in AGNs is still controversial (Done et al., 2012), it is still necessary to investgate the influence of the soft X-ray excess on determining black hole spin. It was done for MCG -06-30-15 which showed a soft excess below ~ 0.7 keV (Brenneman & Reynolds, 2006). Fitting physical models to the broadband spectrum at 2-10 keV with broad iron line, the spin of the black hole in MCG -06-30-15 is well constrained to be $a_* = 0.997$. Moreover, if including the observed features at the lower energy bands 0.6-2 keV and introducing additional components as the possible origin of soft X-ray excess, the best fits to the overall spectrum estimated the black hole spin of $a_* = 0.997$ or 0.989, which indicated the weak influence of the soft X-ray excess on determining the spin of the black hole. Given that we don't have the observation of soft X-ray excess for the five sources in our work, we try to discuss the influence of the soft X-ray excess in terms of power dissipation. We assume that 20% of the dissipated disk power is radiated as soft X-ray excess component (Marinucci et al., 2014), then the parameter f is defined as the ratio of the dissipated power in the corona to the remaining power in the disk, i.e., $f = Q^+_{\rm cor}/(80\% Q^+_{\rm dissi})$. We re-fit the SED of PG 1322+659 with this definition of f, and find that the best-fitting value of black hole spin $a_* = -0.9$, showing small difference in the spin parameter. The remaining model parameters are $f = 0.58$, $\dot{m} = 0.378$, and $\theta = 24.7$, respectively.

For the traditional thin accretion disk model, the mass accretion rate $\dot{m} \lesssim 0.3$ is required in order to satisfy the geometrically thin approximation, i.e., $H_{\rm d}/R \lesssim 0.1$ (e.g., Laor & Netzer, 1989; Esin et al., 1997; King, 2012; Abramowicz & Fragile, 2013). We find that $\dot{m} \gtrsim 0.3$ is required for the spectral fitting in five sources in this work. Our calculations show that the situation is different for the accretion disk with corona, because a fraction of gravitational power is transported into the corona, which reduces the radiation pressure of the disk for a given mass accretion rate $\dot{m}$. In Fig. 13, we find that the geometrically thin disk assumption is still valid even if $0.3 < \dot{m} < 0.5$ when a typical value of $f = 0.5$ is adopted. This implies that the thin accretion disk corona model is applicable for all quasars

in this work. For more luminous quasars with $\dot{m} \gtrsim 0.5$, a general relativistic slim accretion disk corona model is required, which will be reported in our future work.

In this work, we tentatively propose a variant of the continuum-fitting method to constrain the black hole spin parameter a_* in AGNs with a general relativistic accretion corona model. A reliable way to test the feasibility of this proposed method is to apply it to a few stellar-mass black hole X-ray binaries with available estimates of the black hole spin from both continuum-fitting and broad Fe Kα line fitting methods, to see whether the similar results can be obtained. In this paper, it is found that the black hole spin parameter a_* can be well constrained, if the hard X-ray continuum spectrum and the black hole mass are accurately measured. We have not studied the statistics of the black hole spin parameter a_* in this work, due to the small number of the quasars, which can provide useful information when a large sample of quasars with measured black hole spins a_*.

Acknowledgements We thank Zhaohui Shang for the SED data, careful reading the manuscript, and helpful comments/suggestions. Weimin Yuan, Tinggui Wang, Minfeng Gu, Shiying Shen, and Jianmin Wang are thanked for the helpful discussion. Hengxiao Guo is thanked for fitting the emission lines in Fig. 12. This work is supported by the NSFC (grants 11173043, 11121062, 11233006, 11073020, 11373056, and 11473054), the Fundamental Research Funds for the Central Universities (WK2030220004), the CAS/SAFEA International Partnership Program for Creative Research Teams (KJCX2-YW-T23), and Shanghai Municipality.

References

Abramowicz, M. A., & Fragile, P. C. 2013, Living Reviews in Relativity, 16, 1
Alexander, D. M., & Hickox, R. C. 2012, Nature, 56, 93
Antonucci, R. 1999, High Energy Processes in Accreting Black Holes, 161, 193
Arnaud, K. A. 1996, Astronomical Data Analysis Software and Systems V, 101, 17
Barr, P., White, N. E., & Page, C. G. 1985, MNRAS, 216, 65P
Barth, A. J., Pancoast, A., Thorman, S. J., et al. 2011, ApJ, 743, L4
Bechtold, J., Czerny, B., Elvis, M., Fabbiano, G., & Green, R. F. 1987, ApJ, 314, 699
Beloborodov, A. M. 1999, ApJ, 510, L123
Bentz, M. C., Walsh, J. L., Barth, A. J., et al. 2009, ApJ, 705, 199
Blaes, O. 2013, Space Sci. Rev., 58
Blandford, R. D., & Znajek, R. L. 1977, MNRAS, 179, 433
Blandford, R. D., & Payne, D. G. 1982, MNRAS, 199, 883
Berti, E., & Volonteri, M. 2008, ApJ, 684, 822
Brenneman, L. W., & Reynolds, C. S. 2006, ApJ, 652, 1028
Brinkmann, W., Yuan, W., & Siebert, J. 1997, A&A, 319, 413
Calderone, G., Ghisellini, G., Colpi, M., & Dotti, M. 2013, MNRAS, 431, 210
Cao, X. 2009, MNRAS, 394, 207
Chandrasekhar, S. 1960, New York: Dover, 1960,
Chen, L., Cao, X., & Bai, J. M. 2012, ApJ, 748, 119
Chiang, J. 2002, ApJ, 572, 79
Cunningham, C. T. 1975, ApJ, 202, 788
Czerny, B., Hryniewicz, K., Nikołajuk, M., & Sądowski, A. 2011, MNRAS, 415, 2942
Davis, S. W., & Laor, A. 2011, ApJ, 728, 98
de La Calle Pérez, I., Longinotti, A. L., Guainazzi, M., et al. 2010, A&A, 524, A50
Di Matteo, T. 1998, MNRAS, 299, L15
Donato, D., Ghisellini, G., Tagliaferri, G., & Fossati, G. 2001, A&A, 375, 739
Done, C., Davis, S. W., Jin, C., Blaes, O., & Ward, M. 2012, MNRAS, 420, 1848
Done, C., Jin, C., Middleton, M., & Ward, M. 2013, MNRAS, 434, 1955
Dotti, M., Colpi, M., Pallini, S., Perego, A., & Volonteri, M. 2013, ApJ, 762, 68
Esin, A. A., McClintock, J. E., & Narayan, R. 1997, ApJ, 489, 865
Fanali, R., Caccianiga, A., Severgnini, P., et al. 2013, MNRAS, 433, 648

Ferrarese, L., & Merritt, D. 2000, ApJ, 539, L9
Frank, J., King, A., & Raine, D. 1992, Camb. Astrophys. Ser., Vol. 21,,
Galeev, A. A., Rosner, R., & Vaiana, G. S. 1979, ApJ, 229, 318
Ghisellini, G., Padovani, P., Celotti, A., & Maraschi, L. 1993, ApJ, 407, 65
Gilli, R., Comastri, A., & Hasinger, G. 2007, A&A, 463, 79
Goosmann, R. W., Czerny, B., Mouchet, M., et al. 2006, A&A, 454, 741
Gou, L., McClintock, J. E., Reid, M. J., et al. 2011, ApJ, 742, 85
Gou, L., McClintock, J. E., Remillard, R. A., et al. 2014, ApJ, 790, 29
Grupe, D., Thomas, H.-C., & Beuermann, K. 2001, A&A, 367, 470
Haardt, F., & Maraschi, L. 1991, ApJ, 380, L51
Haardt, F., Maraschi, L., & Ghisellini, G. 1994, ApJ, 432, L95
Hirose, S., Blaes, O., & Krolik, J. H. 2009, ApJ, 704, 781
Hopkins, P. F., Hernquist, L., Cox, T. J., & Kereš, D. 2008, ApJS, 175, 356
Hubeny, I., Blaes, O., Krolik, J. H., & Agol, E. 2001, ApJ, 559, 680
Kaspi, S., Smith, P. S., Netzer, H., et al. 2000, ApJ, 533, 631
Kawakatu, N., Imanishi, M., & Nagao, T. 2007, ApJ, 661, 660
King, A. 2012, Mem. Soc. Astron. Italiana, 83, 466
Kishimoto, M., Antonucci, R., Blaes, O., et al. 2008, Nature, 454, 492
Koratkar, A., & Blaes, O. 1999, PASP, 111, 1
Kormendy, J., & Richstone, D. 1995, ARA&A, 33, 581
Kubota, A., Done, C., Davis, S. W., et al. 2010, ApJ, 714, 860
Laor, A., & Netzer, H. 1989, MNRAS, 238, 897
Laor, A. 1991, ApJ, 376, 90
Laor, A., & Davis, S. W. 2014, MNRAS, 60
Li, L.-X., Zimmerman, E. R., Narayan, R., & McClintock, J. E. 2005, ApJS, 157, 335
Li, Y.-R., Wang, J.-M., Ho, L. C., Du, P., & Bai, J.-M. 2013, ApJ, 779, 110
Li, Y.-R., Yuan, Y.-F., Wang, J.-M., Wang, J.-C., & Zhang, S. 2009, ApJ, 699, 513
Lister, M. L. 2001, ApJ, 562, 208
Lister, M. L., Aller, H. D., Aller, M. F., et al. 2009, AJ, 137, 3718
Liu, B. F., Mineshige, S., & Shibata, K. 2002, ApJ, 572, L173
Liu, Y., & Zhang, S. N. 2011, ApJ, 728, L44
Lohfink, A. M., Reynolds, C. S., Miller, J. M., et al. 2012, ApJ, 758, 67
Malkan, M. A., & Sargent, W. L. W. 1982, ApJ, 254, 22
Marconi, A., Risaliti, G., Gilli, R., et al. 2004, MNRAS, 351, 169
Marinucci, A., Matt, G., Miniutti, G., et al. 2014, ApJ, 787, 83
Martocchia, A., Matt, G., Karas, V., Belloni, T., & Feroci, M. 2002, A&A, 387, 215
McClintock, J. E., Narayan, R., Davis, S. W., et al. 2011, Classical and Quantum Gravity, 28, 114009
McConnell, N. J., Ma, C.-P., Gebhardt, K., et al. 2011, Nature, 480, 215
Merloni, A. 2004, MNRAS, 353, 1035
Meyer, F., Liu, B. F., & Meyer-Hofmeister, E. 2000, A&A, 361, 175
Miller, J. M., Fabian, A. C., in't Zand, J. J. M., et al. 2002, ApJ, 577, L15
Miniutti, G., Fabian, A. C., & Miller, J. M. 2004, MNRAS, 351, 466
Moderski, R., & Sikora, M. 1996, MNRAS, 283, 854
Molina, M., Bassani, L., Malizia, A., et al. 2013, MNRAS, 433, 1687
Nandra, K., George, I. M., Mushotzky, R. F., Turner, T. J., & Yaqoob, T. 1997, ApJ, 488, L91
Narayan, R., & Yi, I. 1994, ApJ, 428, L13
Novikov, I. D., & Thorne, K. S. 1973, Black Holes (Les Astres Occlus), 343
Orosz, J. A., Steiner, J. F., McClintock, J. E., et al. 2014, ApJ, 794, 154
Page, D. N., & Thorne, K. S. 1974, ApJ, 191, 499
Page, K. L., Reeves, J. N., O'Brien, P. T., & Turner, M. J. L. 2005, MNRAS, 364, 195
Pancoast, A., Brewer, B. J., & Treu, T. 2011, ApJ, 730, 139
Pancoast, A., Brewer, B. J., Treu, T., et al. 2012, ApJ, 754, 49

Pancoast, A., Brewer, B. J., Treu, T., et al. 2014, MNRAS, 445, 3073
Patrick, A. R., Reeves, J. N., Porquet, D., et al. 2011, MNRAS, 411, 2353
Peterson, B. M., Ferrarese, L., Gilbert, K. M., et al. 2004, ApJ, 613, 682
Porquet, D., Reeves, J. N., O'Brien, P., & Brinkmann, W. 2004, A&A, 422, 85
Qiao, E., & Liu, B. F. 2015, MNRAS, 448, 1099
Remillard, R. A., & McClintock, J. E. 2006, ARA&A, 44, 49
Reynolds, C. S., & Nowak, M. A. 2003, Phys. Rep., 377, 389
Runnoe, J. C., Shang, Z., & Brotherton, M. S. 2013, MNRAS, 435, 3251
Sakimoto, P. J., & Coroniti, F. V. 1981, ApJ, 247, 19
Sambruna, R. M. 1997, ApJ, 487, 536
Schlegel, D. J., Finkbeiner, D. P., & Davis, M. 1998, ApJ, 500, 525
Shafee, R., McClintock, J. E., Narayan, R., et al. 2006, ApJ, 636, L113
Shakura, N. I., & Sunyaev, R. A. 1973, A&A, 24, 337
Shang, Z., Brotherton, M. S., Wills, B. J., et al. 2011, ApJS, 196, 2
Shemmer, O., Brandt, W. N., Netzer, H., Maiolino, R., & Kaspi, S. 2006, ApJ, 646, L29
Shen, Y., Richards, G. T., Strauss, M. A., et al. 2011, ApJS, 194, 45
Shields, G. A. 1978, Nature, 272, 706
Steiner, J. F., McClintock, J. E., Remillard, R. A., Narayan, R., & Gou, L. 2009a, ApJ, 701, L83
Steiner, J. F., Narayan, R., McClintock, J. E., & Ebisawa, K. 2009b, PASP, 121, 1279
Steiner, J. F., McClintock, J. E., Orosz, J. A., et al. 2014, ApJ, 793, L29
Stella, L., & Rosner, R. 1984, ApJ, 277, 312
Sun, W.-H., & Malkan, M. A. 1989, ApJ, 346, 68
Sunyaev, R. A., & Titarchuk, L. G. 1985, A&A, 143, 374
Svensson, R., & Zdziarski, A. A. 1994, ApJ, 436, 599
Taam, R. E., & Lin, D. N. C. 1984, ApJ, 287, 761
Tang, B., Shang, Z., Gu, Q., Brotherton, M. S., & Runnoe, J. C. 2012, ApJS, 201, 38
Vanden Berk, D. E., Richards, G. T., Bauer, A., et al. 2001, AJ, 122, 549
Vasudevan, R. V., & Fabian, A. C. 2007, MNRAS, 381, 1235
Vestergaard, M., & Osmer, P. S. 2009, ApJ, 699, 800
Vestergaard, M., & Peterson, B. M. 2006, ApJ, 641, 689
Volonteri, M., Madau, P., Quataert, E., & Rees, M. J. 2005, ApJ, 620, 69
Wang, J.-M., Watarai, K.-Y., & Mineshige, S. 2004, ApJ, 607, L107
Wills, B. J., & Brotherton, M. S. 1995, ApJ, 448, L81
Woo, J.-H., & Urry, C. M. 2002, ApJ, 581, L5
Wu, Q., Cao, X., Ho, L. C., & Wang, D.-X. 2013, ApJ, 770, 31
Wu, X.-B., Wang, R., Kong, M. Z., Liu, F. K., & Han, J. L. 2004, A&A, 424, 793
You, B., Cao, X., & Yuan, Y.-F. 2012, ApJ, 761, 109
You, B., Czerny, B., Sobolewska, M. et al.: 2015, arXiv:1506.03959
Yuan, W., Liu, B. F., Zhou, H., & Wang, T. G. 2010, ApJ, 723, 508
Zdziarski, A. A., Gierlinski, M., Gondek, D., & Magdziarz, P. 1996, A&AS, 120, 553
Zdziarski, A. A., Lubiński, P., & Smith, D. A. 1999, MNRAS, 303, L11
Zhang, J. L., Xiang, S. P., & Lu, J. F. 1985, Ap&SS, 113, 181
Zhang, S. N., Cui, W., & Chen, W. 1997, ApJ, 482, L155
Zheng, W., Kriss, G. A., Telfer, R. C., Grimes, J. P., & Davidsen, A. F. 1997, ApJ, 475, 469
Zhou, X.-L., & Zhao, Y.-H. 2010, ApJ, 720, L206